Zeng, Zezhu; Zhang, Cunzhi; Xia, Yi; Fan, Zheyong; Wolverton, Chris; Chen, Yue

Nonperturbative phonon scatterings and the two-channel thermal transport in Tl3VSe4

Published in:
Physical Review B

DOI:
10.1103/PhysRevB.103.224307

Published: 01/06/2021

Document Version
Publisher's PDF, also known as Version of record

Please cite the original version:
Zeng, Z., Zhang, C., Xia, Y., Fan, Z., Wolverton, C., & Chen, Y. (2021). Nonperturbative phonon scatterings and the two-channel thermal transport in Tl3VSe4. *Physical Review B*, *103*(22), Article 224307. https://doi.org/10.1103/PhysRevB.103.224307

Nonperturbative phonon scatterings and the two-channel thermal transport in Tl_3VSe_4

Zezhu Zeng [1], Cunzhi Zhang [1], Yi Xia [2], Zheyong Fan [3], Chris Wolverton [2], and Yue Chen [1,4,*]

[1] *Department of Mechanical Engineering, The University of Hong Kong, Pokfulam Road, Hong Kong SAR, China*
[2] *Department of Materials Science and Engineering, Northwestern University, Evanston, Illinois 60208, USA*
[3] *QTF Centre of Excellence, Department of Applied Physics, Aalto University, FI-00076, Aalto, Finland*
[4] *HKU Zhejiang Institute of Research and Innovation, 1623 Dayuan Road, Lin An 311305, China*

(Received 26 January 2021; accepted 4 June 2021; published 21 June 2021)

We study the role of nonperturbative phonon scattering in strongly anharmonic materials having ultralow lattice thermal conductivity with unusual temperature dependence. We take Tl_3VSe_4 as an example and investigate its lattice dynamics using perturbation theory (PT) up to the fourth order and molecular dynamics (MD) with a machine-learning potential. We find distinct differences of phonon linewidth between PT and MD in the whole Brillouin zone. The comparison between the theoretical phonon linewidths and experiments suggests that PT severely underestimates the phonon scatterings, even when the fourth-order anharmonicity is included. Moreover, we extend our calculations to higher temperatures and evaluate the two-channel thermal conductivity based on the unified theory developed by Simoncelli *et al.* [Nat. Phys. **15**, 809 (2019)]. We find a crucial coherence contribution to the total thermal conductivity at high temperatures. Our results pave the path for future studies of phonon properties and lattice thermal conductivities of strongly anharmonic crystals beyond the conventional PT realm.

DOI: 10.1103/PhysRevB.103.224307

I. INTRODUCTION

Many studies [1–7] demonstrate the successes of perturbation theory (PT) and the Boltzmann transport equation (BTE) in exploring the heat conduction of a wide variety of materials. Nevertheless, it is still challenging to reliably and quantitatively understand the unusual phonon properties and ultralow lattice thermal conductivities (κ) of strongly anharmonic materials. The anharmonic lattice dynamics for complicated crystals such as clathrates [8–10] and perovskites [11–14], where the relationship between thermal conductivity and temperature (T) may severely deviate from T^{-1}, may also require more sophisticated theoretical treatments.

In recent years, high-order phonon interactions [5,15–17] and temperature-dependent anharmonic phonon renormalization [2,10,18–21] have been shown to be indispensable to describe the lattice dynamics of materials with strong anharmonicity [22–24]. In addition to these advancements in the perturbation approach, a second thermal transport channel was proposed when the phonon mean free path is smaller than the phonon wavelength or the minimum interatomic spacing in strongly anharmonic or amorphous materials [25–27]. Recently, Mukhopadhyay *et al.* [28] studied thermal transport in Tl_3VSe_4, a promising thermoelectric material that has an ultralow thermal conductivity of 0.30 W/mK at room temperature. A two-channel model by joint consideration of particlelike phonons and wavelike phonons among uncorrelated localized oscillators was applied to explain the ultralow thermal conductivity. They used the Cahill-Watson-Pohl (CWP) model [29] to approximately capture the coherence of acoustic branches as the CWP model only considers the dispersive nature of the acoustic mode carriers. Furthermore, a unified theory of thermal transport in crystals and glasses was also developed by Simoncelli *et al.* [25] to successfully quantify the population (dominated by particlelike phonons) and coherence (dominated by wavelike phonons) terms of the total thermal conductivity in $CsPbBr_3$, a thermoelectric material with an ultralow κ. They derived, from the Wigner phase space formulation of quantum mechanics, a general transport equation that accounts for disorder and anharmonicity simultaneously and includes the coherence contribution[1] from acoustic and optical phonon modes [25,27,30].

However, the intrinsic thermal transport mechanisms of Tl_3VSe_4 are still under debate. Xia *et al.* [31] calculated the coherence contribution to the total thermal conductivity at 300 K using the unified theory based on anharmonic phonon renormalization and four-phonon processes and found that the coherence term is much smaller than the population contribution. This result is different from that of Mukhopadhyay *et al.*, who estimated a coherence part comparable to the part from the particlelike phonons using the CWP model, based on the three-phonon contribution [28]. Jain [32] further developed the state-of-the-art perturbation theory both considering thermal expansion and temperature-dependent force constants for Tl_3VSe_4. Both of these studies are based on PT,

*yuechen@hku.hk

[1] The coherence term here indicates the contribution from off-diagonal terms of lattice thermal conductivity, corresponding to the coherent contribution of phonon modes with the same wave vector but different phonon branches.

however, further evidence is needed to verify whether the anharmonic terms can still be treated perturbatively in strongly anharmonic materials [33,34]. Furthermore, higher-order anharmonic terms beyond the fourth order may become crucial, especially at high temperatures. In-depth understanding of the unusual temperature dependence of thermal conductivity is also of great significance for improving the efficiency of thermoelectric materials. All the above issues prompt us to explore the anharmonic lattice dynamics of Tl_3VSe_4 at higher temperatures beyond the PT framework.

Here, we construct an accurate machine-learning Gaussian approximation potential (GAP) [37–39] for Tl_3VSe_4 based on the first-principles calculations (see Sec. I of Supplemental Material (SM) [40]). Using both PT considering anharmonicity up to the fourth-order and MD simulations, we calculate the phonon properties and lattice thermal conductivity of Tl_3VSe_4. We show that there is a large discrepancy of phonon linewidth between PT and Raman experiment [28] at the Γ point. On the other hand, a significantly improved agreement of linewidths with experiments is obtained via MD simulations. Moreover, the difference of phonon lifetimes from PT and MD in the whole Brillouin zone has been demonstrated at temperatures between 300 K and 500 K. Finally, the two channel thermal conductivity has been calculated based on phonon lifetimes obtained from MD and PT. We find that the coherence contribution is comparable with the population contribution at room temperature and dominates the thermal transport at higher temperatures. Our results show that PT including anharmonicity up to the fourth order may still not be adequate to describe the lattice dynamics of Tl_3VSe_4 at high temperatures. In contrast, MD simulations based on the accurate GAP potential give more reliable results.

II. CONSTRUCTION OF A GAUSSIAN MACHINE-LEARNING POTENTIAL

A $2 \times 2 \times 2$ supercell (128 atoms) was used to perform first-principles molecular dynamics (MD) simulations using VASP [41] and to generate the randomly displaced configurations. An energy cutoff value of 500 eV and a Γ-centering $1 \times 1 \times 1$ k-point mesh were used for the MD simulations. The convergence criterion of energy was set to 10^{-5} eV. The projector augmented wave (PAW) method was used to describe the electron-ion interaction [42]. PBEsol exchange-correlation functional [43] was used as it improves the predicted lattice constants compared with the experimental results [28]. We performed first-principles MD simulations for 12 ps with a timestep of 2 fs at different temperatures (100, 200, 300, 400, and 500 K) and sampled the trajectories by a time interval of 100 fs. A total of 450 configurations were extracted as the initial training data set. Single-point energy calculations were performed to obtain the atomic forces of these configurations with a Γ-centered $2 \times 2 \times 2$ k-point mesh. For more accurate atomic forces, the convergence criterion of energy was enhanced to 10^{-8} eV. After obtaining these first-principles data, we constructed an initial interatomic potential. We used this potential to perform classical MD simulations at 400 and 600 K and extracted 50 configurations as the external iteration training data to refit the potential.

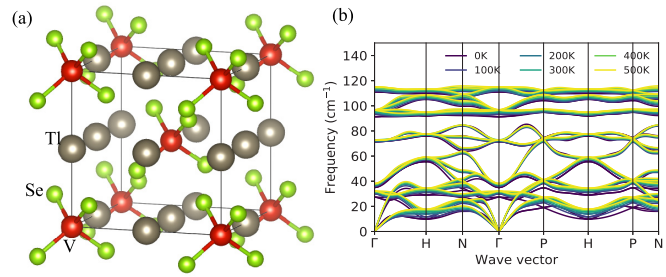

FIG. 1. (a) Crystal structure of Tl_3VSe_4 visualized using VESTA [35]. (b) Phonon dispersions at different temperatures calculated using the self-consistent harmonic Hamiltonian approximation method [36].

Eventually, we obtained 500 configurations to re-train the potential.

For cross validation, we performed classical MD simulations using GAP and obtained 40 random configurations as the validation set at 300 and 600 K. Accurate first-principles calculations were performed to obtain energies and atomic forces for cross validation. The root mean square errors (RMSE) of energy for both of the training and validation data sets are 0.001 eV/Å, and the RMSE of atomic force for the training and validation data sets are 0.039 eV/Å and 0.046 eV/Å, respectively. The cross-validation results are shown in Fig. S1 of SM.

III. CRYSTAL STRUCTURE AND RENORMALIZED PHONON PROPERTIES

The crystal structure of Tl_3VSe_4 is shown in Fig. 1(a). Anharmonic phonon frequency renormalization has been calculated using the self-consistent harmonic approximation method [36,44,45] from 0 to 500 K, and the results are shown in Fig. 1(b). The computational details are included in Sec. III of the SM. It is seen that there is an apparent phonon hardening of the low-frequency modes as temperature increases. These renormalized phonons can lead to different phonon phase space and group velocities, which further affect the phonon lifetimes and thermal conductivity [19,31,46]. Using the temperature dependent phonon frequencies, we can further calculate the phonon lifetimes and thermal conductivity under the PT framework including phonon anharmonicities up to the fourth order based on our implementation of four-phonon scatterings. (see Secs. III and IV of SM for details).

The phonon linewidths calculated from PT for the four Raman-active modes at the Γ point are severely underestimated, comparing to the experimental results (see Table I). The largest difference between the theoretical and experimental linewidths is observed in the A_1 mode, of which the experimental linewidth (0.75 ps^{-1}) is much larger than the theoretical value from PT (0.14 ps^{-1}). On the other hand, the corresponding phonon linewidth obtained from MD simulations is significantly improved (0.44 ps^{-1}). The PT linewidth (0.66 ps^{-1}) of the high-frequency T_2 mode is also smaller than the experimental value (0.81 ps^{-1}). These linewidth differences of A_1 and the high-frequency T_2 modes may be related to the requirement of energy conservation in

TABLE I. Experimental [28] and theoretical phonon frequencies and linewidths of the four Raman-active phonon modes at the Γ point at 300 K.

	Frequency (cm^{-1})			Linewidth (ps^{-1})		
Symmetry	SCP	Expt.	MD	PT_3+4	Expt.	MD
T_2	31.4	33.2	32.7	0.33	1.26	0.90
E	95.2	94.7	97.7	0.60	1.39	1.04
A_1	231.8	219.8	219.8	0.14	0.75	0.44
T_2	364.8	365.9	365.4	0.66	0.81	0.80

PT limits three-phonon scattering channels [47], especially for those modes with restricted phase space (see Fig. S4 of SM). It was pointed out [48] that MD simulations can naturally include inelastic scattering processes that may lead to a better agreement between the MD and the experimental phonon linewidths for the isolated A_1 and high-frequency T_2 optical phonon modes, which have a sizable frequency gap from other modes. It is also noted that the phonon frequency of A_1 mode obtained from the self-consistent method is larger than the results from MD and Raman experiment, which may be related to the systematic errors in the self-consistent phonon method as discussed in a previous study [49].

Furthermore, phonon linewidths of the other two Raman-active modes obtained from PT are also much smaller than the experimental values although the phase space is not restricted. For instance, the experimental linewidth of the low-frequency T_2 mode (1.26 ps^{-1}) is approximately four times larger than the PT linewidth (0.33 ps^{-1}). On the contrary, MD simulations (0.90 ps^{-1}) give a better agreement with the experiment. Therefore, even including the fourth-order anharmonicity, PT may still be insufficient to describe the lattice dynamics of strongly anharmonic materials with ultralow lattice thermal conductivity, such as Tl_3VSe_4. Under higher temperatures, the anharmonic contributions become more important. It is thus expected that the results obtained from PT may deviate further from experiments.

The phonon linewidths across the Brillouin zone are shown in Fig. 2 (see Fig. S7 of SM for results including the high-frequency optical modes). We find an apparent difference of linewidth between PT and MD across the Brillouin zone, and the difference becomes more distinct at higher temperatures. For the phonon modes with frequency under 15 cm^{-1}, it is apparent that the linewidths obtained from MD simulations are larger than those from PT considering up to four-phonon interactions, especially at 500 K. Because the low-frequency acoustic phonon modes dominate the lattice thermal conductivity, we expect that the thermal transport of Tl_3VSe_4 may be strongly affected when nonperturbative phonon scatterings are considered.

IV. LATTICE THERMAL CONDUCTIVITY

We have calculated the lattice thermal conductivity of Tl_3VSe_4 using the sinusoidal approach-to-equilibrium molecular dynamics (SAEMD) [50,51] based on our machine learning GAP potential. This method can be used to conveniently calculate the lattice thermal conductivity because it directly simulates the heat transport process by following Fourier's law and has no approximation to the heat carriers (see Sec. IV C of SM for details). The lattice thermal conductivities obtained from SAEMD are in good agreement with experiments (see Fig. 3 and Fig. S8 of SM). We can use the results of lattice thermal conductivity from SAEMD as a benchmark to have a contrast with the results based on BTE at high temperatures.

The phonon lifetimes (reciprocal of linewidths) obtained from PT have been used to calculate the population and coherence terms of the lattice thermal conductivity based on the BTE (see Secs. IV A and IV B of SM for details). It is seen from Fig. 3(a), where the lattice thermal conductivities are calculated using the PT lifetimes, that the coherence contribution is equal to 0.09 W/mK at 300 K, consistent with the result of Xia *et al.* (0.08 W/mK) [31]. Population lattice thermal conductivity calculated from PT at 300 K is equal to 0.29 W/mK, which is also in excellent agreement with the result obtained by Xia *et al.* [31]. The population

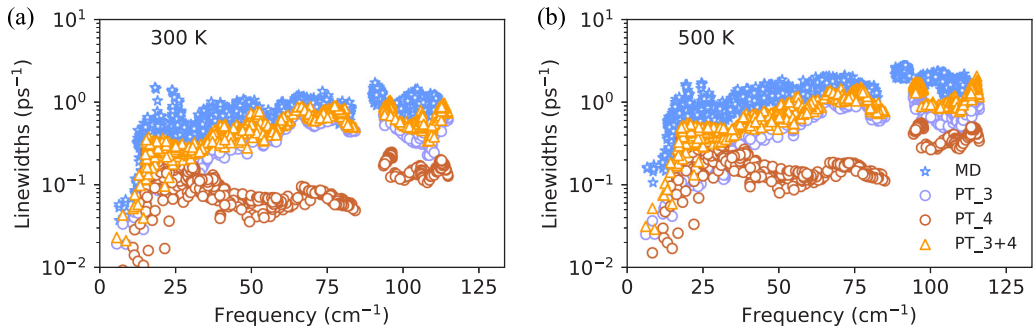

FIG. 2. Theoretical phonon linewidths calculated from MD and PT at different temperatures. PT_3, PT_4, and PT_3+4 represent the phonon linewidths computed from perturbation theory considering three-phonon, four-phonon, and both three- and four-phonon scatterings, respectively.

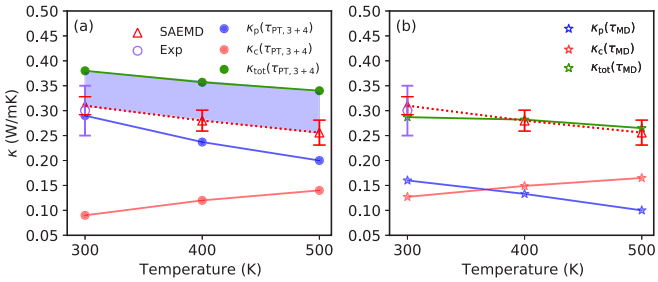

FIG. 3. Population and coherence contributions calculated based on phonon lifetimes obtained from PT considering third- and fourth-order anharmonic terms (a) and from MD simulations using a machine learning GAP potential (b). The experimental thermal conductivity at 300 K and the SAEMD results are also shown for comparisons. The blue shaded region shows the difference between the BTE lattice thermal conductivity calculated using the PT phonon lifetimes and that obtained from SAEMD simulation.

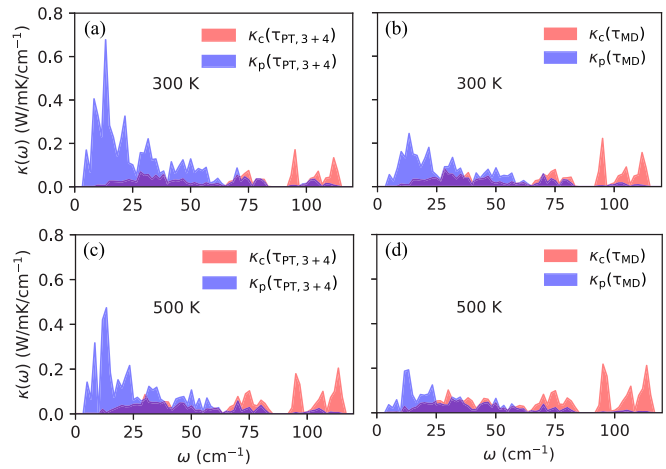

FIG. 4. The spectral population (κ_p) and coherence (κ_c) contributions to the lattice thermal conductivity calculated from BTE using the PT and MD phonon lifetimes

contribution is much larger than the coherence contribution at 300 K. Thus, the population contribution dominates the thermal transport of Tl_3VSe_4 at 300 K under the PT framework. However, the total thermal conductivity calculated using the PT lifetimes is obviously higher than the experiments (0.30 W/mK) [28] and SAEMD results (0.31 W/mK). The differences between the lattice thermal conductivities calculated using the PT lifetimes and those from SAEMD become even larger at 400 K and 500 K. For instance, the κ_{tot} from SAEMD is 0.25 W/mK at 500 K, while the BTE κ_{tot} based on $\tau_{PT,3+4}$ is 0.35 W/mK (0.20 W/mK from the population channel and 0.15 W/mK from the coherence channel). Thus, the total lattice thermal conductivity is overestimated by 40% within the BTE scheme taking the PT phonon lifetimes at 500 K. We exclude the contributions of boundary and isotope scatterings as they were shown to be insignificant in Tl_3VSe_4 at high temperatures [28,31].

Because the overestimated thermal conductivity from BTE may be related to the inaccurate PT phonon lifetimes, we have further calculated the lattice thermal conductivities using phonon lifetimes obtained from MD simulations based on our machine learning GAP potential (see Sec. II of SM for the extraction of τ_{MD}). It is seen from Fig. 3(b) that the population contribution to the total thermal conductivity becomes much smaller because of the shorter MD lifetimes. However, once the coherence contribution is considered, good agreement is obtained with the experimental value at 300 K and the SAEMD simulations at higher temperatures. Based on the phonon lifetimes obtained from MD simulations, we see that the coherence contribution is comparable with the population contribution at 300 K. At 400 and 500 K, the coherence contribution becomes even larger than the population contribution to the lattice thermal conductivity. Our results indicate that the coherence channel is important in describing the lattice thermal transport of Tl_3VSe_4, especially at high temperatures. We have also calculated the two channel thermal conductivity based on τ_{MD} in the low temperature region from 100 to 250 K, and the results agree well with the experimental data (see Fig. S8 of SM). The coherence contribution becomes much smaller at low temperatures, e.g., $\kappa_c(\tau_{MD})$ is equal to 0.04 W/mK at 100 K and may be negligible.

The spectral lattice thermal conductivity is shown in Fig. 4 to further understand the temperature dependencies of the population and coherence contributions. It is apparent from Fig. 4(a) that $\kappa_p(\tau_{PT,3+4})$ governs the heat transport of Tl_3VSe_4 at 300 K owing to the phonons in the low-frequency regime (0–75 cm^{-1}). In Fig. 4(c), there is an evident decrease of $\kappa_p(\tau_{PT,3+4})$ and increase of $\kappa_c(\tau_{PT,3+4})$ at 500 K. However, if phonon lifetimes obtained from MD (τ_{MD}) are used to calculate the lattice thermal conductivity, $\kappa_p(\tau_{MD})$ becomes much smaller at 300 K because of the smaller τ_{MD}. As a result, $\kappa_c(\tau_{MD})$ becomes comparable to $\kappa_p(\tau_{MD})$ at 300 K and surpasses $\kappa_p(\tau_{MD})$ at 500 K. We also find the coherence term is rather significant for phonon modes with frequencies near 100 cm^{-1}, which may be attributed to the short lifetimes and the tight bunching of these optical phonon modes. The considerable coherence contribution from optical phonon modes indicates their importance in thermal transport compared with acoustic modes and also reveal the limitation of the CWP model that only considers the coherence from acoustic modes.

V. DISCUSSION

The differences between PT and MD phonon lifetimes may be related to the many flat phonon branches in the low-frequency region where anharmonic phonon properties (frequency shift and linewidth) can be comparable or larger than the harmonic frequency, whereas it is known that PT requires that the perturbative terms must be significantly smaller than the eigenvalues [34,52–54]. For example, the lowest frequencies at the H point are equal to 10.5 cm^{-1} and 19.2 cm^{-1} at 0 and 500 K, respectively. The frequency shift is comparable to the harmonic frequency. Furthermore, a perturbative treatment of the anharmonic terms in Tl_3VSe_4 may not be accurate because of the large thermal displacements of Tl atoms and the weak atomic bonding between Tl and other constituents [28]. Additionally, different from PT, in which we only consider the third- and fourth-order terms, the machine learning GAP potential for MD simulations takes into account

full anharmonicity up to any arbitrary orders. The deficiency of PT in predicting the phonon lifetimes of strongly anharmonic systems at high temperatures due to the absence of high-order perturbative terms has been pointed out in previous studies [33,55,56]. Artús *et al.* also claimed that fifth-order phonon scatterings are crucial for understanding the experimental results of the transverse optical phonon properties in InP [57].

It is noted that the nonperturbative phonon scatterings are not system specific and may exist in a range of materials with strong lattice anharmonicity and ultralow lattice thermal conductivity at high temperatures. We take PbTe and *Cmcm*-SnSe as examples to further demonstrate our conclusions. Computational results of phonon lifetimes, and population and coherence contributions to the lattice thermal transports of PbTe and *Cmcm*-SnSe, are included in SM (see Fig. S11 and Fig. S12). The good agreement of the two channel thermal conductivity of PbTe calculated based on τ_{MD} and $\tau_{\mathrm{PT,34}}$ (Fig. S11c) indicates there are no distinct nonperturbative phonon scatterings in PbTe below 700 K. However, it is seen from Fig. S12 that in *Cmcm*-SnSe, the nonperturbative phonon scatterings are crucial for the phonon linewidths across the Brillouin zone at 900 K, similar to Tl_3VSe_4. These nonperturbative phonon scatterings also significantly decrease the population lattice thermal conductivity (Fig. S12b) and increase the coherence contribution in *Cmcm*-SnSe. These results further support our conclusion that nonperturbative phonon scatterings are important to correctly understand the thermal transport behaviors of strongly anharmonic materials with ultralow lattice thermal conductivity.

VI. CONCLUSION

In summary, PT including anharmonicity up to the fourth order and MD simulations with a first-principles machine-learning GAP potential have been applied to investigate the lattice dynamics of Tl_3VSe_4 at elevated temperatures. We show the phonon linewidths obtained from PT strongly deviate from Raman experiment, while the results obtained from MD simulations agree more reasonably. Using the unified theory and the MD phonon linewidths, we find that the coherence contribution to the lattice thermal conductivity is significant and becomes even larger than the conventional population contribution above 400 K. Our results suggest that PT may not be adequate to describe the strongly anharmonic Tl_3VSe_4 even phonon renormalization and four-phonon processes are considered. In contrast, MD simulations with accurate first-principles machine-learning potentials provide an alternative route to study the lattice dynamics and thermal transport of strongly anharmonic crystals at high temperatures.

ACKNOWLEDGMENTS

This work is supported by the National Natural Science Foundation of China (11874313), the Zhejiang Provincial Natural Science Foundation (LR19A040001), the Research Grants Council of Hong Kong (17201019 and 17300018), and the National Key Research and Development Program of China (2019YFA0209904). Y.X. and C.W. acknowledge financial supports from the Department of Energy, Office of Science, Basic Energy Sciences under Grant DE-SC0014520 (theory of anharmonic phonons). The authors are grateful for the research computing facilities offered by ITS, HKU.

[1] A. Togo, L. Chaput, and I. Tanaka, Distributions of phonon lifetimes in brillouin zones, Phys. Rev. B **91**, 094306 (2015).

[2] T. Tadano and S. Tsuneyuki, Quartic Anharmonicity of Rattlers and Its Effect on Lattice Thermal Conductivity of Clathrates from First Principles, Phys. Rev. Lett. **120**, 105901 (2018).

[3] L. Lindsay and D. Broido, Three-phonon phase space and lattice thermal conductivity in semiconductors, J. Phys.: Condens. Matter **20**, 165209 (2008).

[4] L. Lindsay, D. A. Broido, and T. Reinecke, First-Principles Determination of Ultrahigh Thermal Conductivity of Boron Arsenide: A Competitor for Diamond? Phys. Rev. Lett. **111**, 025901 (2013).

[5] T. Feng, L. Lindsay, and X. Ruan, Four-phonon scattering significantly reduces intrinsic thermal conductivity of solids, Phys. Rev. B **96**, 161201(R) (2017).

[6] A. J. H. McGaughey and M. Kaviany, Quantitative validation of the boltzmann transport equation phonon thermal conductivity model under the single-mode relaxation time approximation, Phys. Rev. B **69**, 094303 (2004).

[7] X. Qian, J. Zhou, and G. Chen, Phonon-engineered extreme thermal conductivity materials, Nat. Mater. **20**, 1 (2021).

[8] C. Chen, Z. Zhang, and J. Chen, Revisit to the impacts of rattlers on thermal conductivity of clathrates, Front. Energy Res. **6**, 34 (2018).

[9] M. Ikeda, H. Euchner, X. Yan, P. Tomeš, A. Prokofiev, L. Prochaska, G. Lientschnig, R. Svagera, S. Hartmann, E. Gati *et al.*, Kondo-like phonon scattering in thermoelectric clathrates, Nat. Commun. **10**, 1 (2019).

[10] T. Tadano, Y. Gohda, and S. Tsuneyuki, Impact of Rattlers on Thermal Conductivity of a Thermoelectric Clathrate: A First-Principles Study, Phys. Rev. Lett. **114**, 095501 (2015).

[11] J. Klarbring, O. Hellman, I. A. Abrikosov, and S. I. Simak, Anharmonicity and Ultralow Thermal Conductivity in Lead-Free Halide Double Perovskites, Phys. Rev. Lett. **125**, 045701 (2020).

[12] J.-Q. Yan, J.-S. Zhou, and J. B. Goodenough, Unusually Strong Orbit-Lattice Interactions in the RVO_3 Perovskites, Phys. Rev. Lett. **93**, 235901 (2004).

[13] W. Lee, H. Li, A. B. Wong, D. Zhang, M. Lai, Y. Yu, Q. Kong, E. Lin, J. J. Urban, J. C. Grossman *et al.*, Ultralow thermal conductivity in all-inorganic halide perovskites, Proc. Natl. Acad. Sci. USA **114**, 8693 (2017).

[14] J.-H. Pöhls and A. Mar, Thermoelectric properties of inverse perovskites A_3TtO (A = Mg, Ca; Tt = Si, Ge): Computational

and experimental investigations, J. Appl. Phys. **126**, 025110 (2019).
[15] T. Feng and X. Ruan, Quantum mechanical prediction of four-phonon scattering rates and reduced thermal conductivity of solids, Phys. Rev. B **93**, 045202 (2016).
[16] T. Feng and X. Ruan, Four-phonon scattering reduces intrinsic thermal conductivity of graphene and the contributions from flexural phonons, Phys. Rev. B **97**, 045202 (2018).
[17] N. K. Ravichandran and D. Broido, Phonon-Phonon Interactions in Strongly Bonded Solids: Selection Rules and Higher-Order Processes, Phys. Rev. X **10**, 021063 (2020).
[18] C. W. Li, O. Hellman, J. Ma, A. F. May, H. B. Cao, X. Chen, A. D. Christianson, G. Ehlers, D. J. Singh, B. C. Sales, O. Delaire *et al.*, Phonon Self-Energy and Origin of Anomalous Neutron Scattering Spectra in SnTe and PbTe Thermoelectrics, Phys. Rev. Lett. **112**, 175501 (2014).
[19] Y. Xia, Revisiting lattice thermal transport in PbTe: The crucial role of quartic anharmonicity, Appl. Phys. Lett. **113**, 073901 (2018).
[20] O. Hellman and I. A. Abrikosov, Temperature-dependent effective third-order interatomic force constants from first principles, Phys. Rev. B **88**, 144301 (2013).
[21] Z. Zeng, S. Li, T. Tadano, Y. Chen *et al.*, Anharmonic lattice dynamics and thermal transport of monolayer InSe under equibiaxial tensile strains, J. Phys.: Condens. Matter **32**, 475702 (2020).
[22] E. Akkermans and R. Maynard, Weak localization and anharmonicity of phonons, Phys. Rev. B **32**, 7850 (1985).
[23] X. He, D. Bansal, B. Winn, S. Chi, L. Boatner, and O. Delaire, Anharmonic Eigenvectors and Acoustic Phonon Disappearance in Quantum Paraelectric $SrTiO_3$, Phys. Rev. Lett. **124**, 145901 (2020).
[24] I. Errea, F. Belli, L. Monacelli, A. Sanna, T. Koretsune, T. Tadano, R. Bianco, M. Calandra, R. Arita, F. Mauri *et al.*, Quantum crystal structure in the 250-kelvin superconducting lanthanum hydride, Nature (London) **578**, 66 (2020).
[25] M. Simoncelli, N. Marzari, and F. Mauri, Unified theory of thermal transport in crystals and glasses, Nat. Phys. **15**, 809 (2019).
[26] Y. Luo, X. Yang, T. Feng, J. Wang, and X. Ruan, Vibrational hierarchy leads to dual-phonon transport in low thermal conductivity crystals, Nat. Commun. **11**, 2554 (2020).
[27] R. Hanus, J. George, M. Wood, A. Bonkowski, Y. Cheng, D. L. Abernathy, M. E. Manley, G. Hautier, G. J. Snyder, and R. P. Hermann, Uncovering design principles for amorphous-like heat conduction using two-channel lattice dynamics, Mater. Today Phys. **18**, 100344 (2021).
[28] S. Mukhopadhyay, D. S. Parker, B. C. Sales, A. A. Puretzky, M. A. McGuire, and L. Lindsay, Two-channel model for ultralow thermal conductivity of crystalline Tl_3VSe_4, Science **360**, 1455 (2018).
[29] D. G. Cahill, S. K. Watson, and R. O. Pohl, Lower limit to the thermal conductivity of disordered crystals, Phys. Rev. B **46**, 6131 (1992).
[30] L. Isaeva, G. Barbalinardo, D. Donadio, and S. Baroni, Modeling heat transport in crystals and glasses from a unified lattice-dynamical approach, Nat. Commun. **10**, 1 (2019).
[31] Y. Xia, K. Pal, J. He, V. Ozoliņš, and C. Wolverton, Particlelike Phonon Propagation Dominates Ultralow Lattice Thermal Conductivity in Crystalline Tl_3VSe_4, Phys. Rev. Lett. **124**, 065901 (2020).
[32] A. Jain, Multichannel thermal transport in crystalline Tl_3VSe_4, Phys. Rev. B **102**, 201201(R) (2020).
[33] J. W. L. Pang, W. J. L. Buyers, A. Chernatynskiy, M. D. Lumsden, B. C. Larson, and S. R. Phillpot, Phonon Lifetime Investigation of Anharmonicity and Thermal Conductivity of UO_2 by Neutron Scattering and Theory, Phys. Rev. Lett. **110**, 157401 (2013).
[34] T. Tadano and S. Tsuneyuki, First-principles lattice dynamics method for strongly anharmonic crystals, J. Phys. Soc. Jpn. **87**, 041015 (2018).
[35] K. Momma and F. Izumi, VESTA: A three-dimensional visualization system for electronic and structural analysis, J. Appl. Crystallogr. **41**, 653 (2008).
[36] I. Errea, M. Calandra, and F. Mauri, Anharmonic free energies and phonon dispersions from the stochastic self-consistent harmonic approximation: Application to platinum and palladium hydrides, Phys. Rev. B **89**, 064302 (2014).
[37] A. P. Bartók, M. C. Payne, R. Kondor, and G. Csányi, Gaussian Approximation Potentials: The Accuracy of Quantum Mechanics, Without the Electrons, Phys. Rev. Lett. **104**, 136403 (2010).
[38] A. P. Bartók, R. Kondor, and G. Csányi, On representing chemical environments, Phys. Rev. B **87**, 184115 (2013).
[39] W. J. Szlachta, A. P. Bartók, and G. Csányi, Accuracy and transferability of gaussian approximation potential models for tungsten, Phys. Rev. B **90**, 104108 (2014).
[40] See Supplemental Material at http://link.aps.org/supplemental/10.1103/PhysRevB.103.224307 for the construction of GAP, the extraction of interatomic force constants, calculation details of lattice thermal conductivity of Tl_3VSe_4, and supplemental results of phonon linewidth and lattice thermal conductivity for PbTe and *cmcm*-SnSe.
[41] G. Kresse and J. Furthmüller, Efficient iterative schemes for ab initio total-energy calculations using a plane-wave basis set, Phys. Rev. B **54**, 11169 (1996).
[42] P. E. Blöchl, Projector augmented-wave method, Phys. Rev. B **50**, 17953 (1994).
[43] J. P. Perdew, A. Ruzsinszky, G. I. Csonka, O. A. Vydrov, G. E. Scuseria, L. A. Constantin, X. Zhou, and K. Burke, Phys. Rev. Lett. **101**, 239702 (2008).
[44] T. R. Koehler, Theory of the Self-Consistent Harmonic Approximation with Application to Solid Neon, Phys. Rev. Lett. **17**, 89 (1966).
[45] N. Werthamer, Self-consistent phonon formulation of anharmonic lattice dynamics, Phys. Rev. B **1**, 572 (1970).
[46] Y. Xia, V. Ozolins, and C. Wolverton, Microscopic Mechanisms of Glass-Like Lattice Thermal Transport in Cubic $Cu_{12}Sb_4S_{13}$ Tetrahedrites, Phys. Rev. Lett. **125**, 085901 (2020).
[47] C. Zhang, Z. Zeng, Q. Sun, and Y. Chen, Hidden energy non-conserved three-phonon scatterings in materials with restricted phase space (unpublished).
[48] A. Raj and J. Eapen, Deducing phonon scattering from normal mode excitations, Sci. Rep. **9**, 7982 (2019).
[49] E. Metsanurk and M. Klintenberg, Sampling-dependent systematic errors in effective harmonic models, Phys. Rev. B **99**, 184304 (2019).
[50] E. Lampin, P. Palla, P.-A. Francioso, and F. Cleri, Thermal conductivity from approach-to-equilibrium molecular dynamics, J. Appl. Phys. **114**, 033525 (2013).

[51] M. Puligheddu, F. Gygi, and G. Galli, First-principles simulations of heat transport, Phys. Rev. Materials **1**, 060802(R) (2017).

[52] M. Lazzeri, M. Calandra, and F. Mauri, Anharmonic phonon frequency shift in MgB_2, Phys. Rev. B **68**, 220509(R) (2003).

[53] K. Esfarjani and Y. Liang, Thermodynamics of anharmonic lattices from first-principles, Nanoscale Energy Transport **7** (2019).

[54] S. Baroni, S. De Gironcoli, A. Dal Corso, and P. Giannozzi, Phonons and related crystal properties from density-functional perturbation theory, Rev. Mod. Phys. **73**, 515 (2001).

[55] A. Glensk, B. Grabowski, T. Hickel, J. Neugebauer, J. Neuhaus, K. Hradil, W. Petry, and M. Leitner, Phonon Lifetimes Throughout the Brillouin Zone at Elevated Temperatures from Experiment and Ab Initio, Phys. Rev. Lett. **123**, 235501 (2019).

[56] Y. Xia, V. I. Hegde, K. Pal, X. Hua, D. Gaines, S. Patel, J. He, M. Aykol, and C. Wolverton, High-Throughput Study of Lattice Thermal Conductivity in Binary Rocksalt and Zinc Blende Compounds Including Higher-Order Anharmonicity, Phys. Rev. X **10**, 041029 (2020).

[57] L. Artús, R. Cuscó, J. R. Martin, and G. González-Díaz, Up to fifth-order raman scattering of InP under nonresonant conditions, Phys. Rev. B **50**, 11552 (1994).